Thermal Field in a NMR Cryostat

A. D'Orazio[1], C. Agostini[*1], S. Fiacco[1]
[1]Università La Sapienza Di Roma – Dipartimento di. Ingegneria Astronautica, Elettrica ed Energetica
*Corresponding author: annunziata.dorazio@uniroma1.it chy.agostini@gmail.com simone.fiacco@gmail.com

Abstract

In this paper, we present the preliminary results about the thermal field inside the cryostat, obtained by finite element numerical simulations performed in Comsol Multiphysics environment. The simulations concern simplified three-dimensional geometries obtained from field inspections and construction schemes; sizes and materials actually used and all modes of heat transfer are taken in account. We discuss some configurations of thermal insulation and boundary conditions able to simulate the effect of a "cold head" placed in contact with a very limited portion of the cryoshields. Finally, we show results about the thermal field when tie rods are mounted that in real cryostats allow to mantain the empty cavity and to center the magnetic field.

Keywords: NMR superconducting magnet, thermal field, cryostat, cold head, DAM sheets.

1. Introduction

Currently, the nuclear magnetic resonance is the technique most widely used in the medical field to obtain images of the inside of the human body, thanks to its alleged ability to not generate damage inside the biological tissue under investigation.Fundamental component of the NMR tomograph is the magnet. By using the property of superconductivity [1], it is possible to achieve an induction field extremely homogeneous, stable and high, ensuring both the formation of an excellent diagnostic image, and the possibility to disable the power to the magnet, avoiding energy costs. To maintain the superconducting alloy (60%Nb - 40%Ti) below the critical temperature T_c (7.2K), the coils are immersed in liquid helium at 4K, within a cryostat. In order to reduce the incoming heat flux and to decrease the amount of evaporated helium, the cryostat is a Dewar vessel for which only conductive and radiative heat transfer occurs. In combination with an effective insulation system, radiative shields are used. They are maintained between 20K and 80K by a "cold head" (Stirling cooler or "pulse tube" with two refrigerating stages), to reduce the temperature gradient in the cryostat. In the Zero Boil-Off configuration, the Pulse Tube Refrigerator [2] is used with two refrigerating stages, the first to maintain a cryo-shield at 50K, the other to keep at 4K the inner wall of the cryogenic tank. In this work, simulations were performed in Comsol Multiphysics environment to analyze the thermal field in cryostat.

2. Structure and technology of cryostat

The main task of the cryostat is to keep the helium in liquid phase (T=4K). The cryostat is constituted by a concentric structure coaxial with the superconducting windings and it is composed, generally, by four vessels, as shown in figure 1: the inner vessel (0.625 cm thick) contains helium, the outer one (0.450 cm thick) is in contact with the ambient air; in the cavity between them (4.424 cm), in which the vacuum is made, there are two intermediate vessels (aluminum radiative shields with emissivity equal to 0.1), maintained at 80 and 20 K, 0.625 cm and 0.40 cm thick respectively. It could be noted that without these cryo-shields the temperature jump through the empty gap would be of order of 290K.

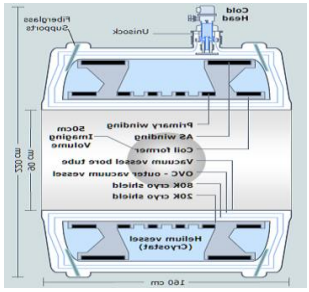

Figure 1. Cryostat's scheme with cryo-shields and cold head [3].

Figure 2. Real Cryostat

To further reduce the radiative heat transfer between the external environment and the liquid helium, some sheets of DAM (Double Aluminized Mylar), each 10μm thick and with emissivity equal to 0.03, are placed into more external empty cavity (1.141 cm thick), through which occurs a higher temperature jump (between ambient air and 80K).

3. Numerical study of the thermal field in cryostat

A preliminary assessment has been focused on the geometrical aspects; three different models of cryostat (shown in figures 3-5) have been implemented, with particular reference to the type of closures placed at the ends. No relevant differences were revealed in the simulation results, at this level of approximation, so that only the case of flat closures will be presented in the following.

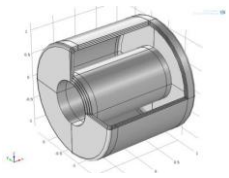

Figure 3. Geometry with flat closures.

Figure 4. Geometry with inclined closures.

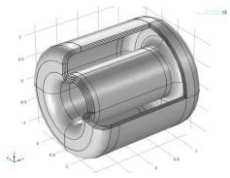

Figure 5. Geometry with rounded closures.

Successively, the thermal boundary conditions were analyzed and implemented. Nusselt number and convective heat transfer coefficients, both for air and liquid helium, were computed iteratively by Matlab software by means of empirical correlations dependent on geometry. More specifically, for the outer steel vessel, composed by two concentric cylinders and vertical closures, the Churchill-Chu correlation [4], holding for natural convection, has been used for lateral surfaces, with cylinder's diameter as characteristic length, as follows

$$Nu = \left\{ 0.6 + \frac{0.387 Ra^{1/6}}{\left[1 + \left(\frac{0.559}{\mathrm{Pr}} \right)^{9/16} \right]^{8/27}} \right\}^2$$

Two heat transfer coefficients for internal and external cylinders result as

$$h_{ext} = 2.13 \frac{W}{m^2 K} \qquad h_{\mathrm{int}} = 2.23 \frac{W}{m^2 K}$$

With regard to vertical closures, the convective coefficients has been computed by means of internal function into Comsol library.
With regard to the internal vessel (figure 6), in the upper part a thermal flux with helium vapor phase was considered.

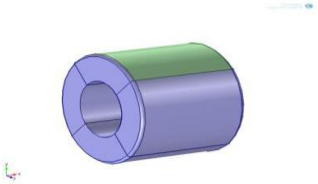

Figure 6. Convective Exchange surfaces with helium (internal steel vessel).

To evaluate the Nusselt number, the following correlation [5] for horizontal plate has been used, because of the high radius of curvature:

$$Nu = 0.15 Ra^{1/3} \qquad Ra > 10^7$$

For remaining part of the internal vessel surfaces, in contact with liquid helium, correlation [5] for coaxial horizontal cylinders (with the gap between the cylinders characteristic length) has been used as follows

$$Nu = 0.4 Ra^{0.20} \qquad 10^6 < Ra < 10^8$$

Two heat transfer coefficients result

$$h_{i\_liq} = 1.30 \frac{W}{m^2 K} \qquad h_{i\_vap} = 4.5 \frac{W}{m^2 K}$$

3.1 Simulation without DAM

At first, simulations have been carried out in case of empty cavity, without DAM's sheet. Results are shown in the following Table 1, in terms of heat fluxes and mean temperatures.

Table 1. Thermal fluxes and mean temperatures without DAM.

Surfaces	**Fluxes [W]**		**Specific fluxes [$\frac{W}{m^2}$]**		**Mean T [K]**
	Radiative	Convective	Radiative	Convective	Radiative
External surface external steel vessel	-226.04	-473.71	-8.36	-17.53	285.53
Internal surface external steel vessel	698.66	0	26.01	0	285.52
External surface external alu vessel	-698.42	0	-26.97	0	80
Internal surface external alu vessel	3.06	0	0.12	0	80
External surface internal alu vessel	-3.06	0	-0.12	0	20
Internal surface internal alu vessel	0.011	0	4.66e-4	0	20
External surface internal steel vessel	-0.011	0	-4.84e-4	0	4.20035
Internal surface internal steel vessel	0	0.011	0	4.89e-4	4.20034

The radiative net heat flux received by the shield maintained at 80K, is very high and not sustainable by any commercial cold head.

3.2 Simulation with DAM

With regard to the DAM sheets, a perfect shielding effect would be obtained with separated DAM sheets, avoiding any contact among them.
At first, this ideal case, for which no contact resistance takes place, has been analyzed, by considering a single sheet with an effective emissivity taking in account the effect of 60 DAM sheets. The results show a considerable decrease of heat flux entering the external aluminum vessel, from 698.42 to 2.985 W.
Actually, among the sheets surely exist some contact points, that constitute conductive paths for the heat transfer and decrease the insulation.
Thus a more realistic model was analyzed in Matlab, in which, in addition to the radiative contribution, a further conductive term was considered.

In this way, it was possible to evaluate a new effective emissivity (Table 2) that takes into account this effect.

Table 2. Effective emissivity

Ideal case	Real case
0.0005257	0.001506

Results of simulations are shown in Table 3.

Table 3. Thermal fluxes and mean temperature with real DAM.

Surfaces	Fluxes $[W]$		Specific fluxes $\left[\frac{W}{m^2}\right]$		Mean T $[K]$
	Radiative	Convective	Radiative	Convective	Radiative
External surface external steel vessel	-3.38	-4.81	-0.13	-0.18	293.04
Internal surface external steel vessel	8.21	0	0.31	0	293.04
External surface DAM	-8.15	0	-0.31	0	247.19
Internal surface DAM	8.15	0	0.31	0	246.89
External surface external alu vessel	-8.12	0	-0.31	0	80
Internal surface external alu vessel	3.06	0	0.12	0	80
External surface internal alu vessel	-3.06	0	-0.12	0	20
Internal surface internal alu vessel	0.011	0	4.66e-4	0	20
External surface internal steel vessel	-0.011	0	-4.85e-4	0	4.20035
Internal surface internal steel vessel	0	0.011	0	4.90e-4	4.20034

3.3 Simulation with cold head

In the following, simulation results regarding the effect of a cold head, are discussed.
The cold head, shown in figure 7, is modeled as two copper plates (4.12 cm diameter and 2.06 cm diameter), simulating two refrigerant stages of a pulse tube, put in contact with two cryo-shields (figure 8).

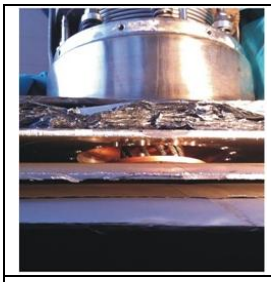

Figure 7. Real cold head.

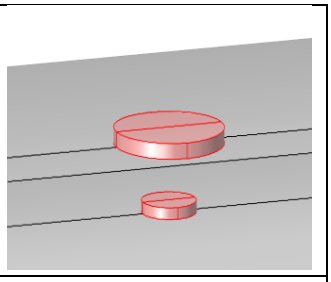

Figure 8. Two copper plate on cryo-shields.

With regard to thermal boundary conditions, the case of imposed heat flux, at the contact surfaces between the cold head and the radiative shields, and the case of imposed temperatures at this surfaces have been considered.
The imposed heat flux, to be removed by the refrigerating stage through each contact surface, was set as equal to the overall difference between the incoming and outgoing flux from the shield (Table 3). For the second case, the imposed temperatures at the cold head surfaces was 80K and 20K respectively. In case of imposed heat flux, temperature fields for external and internal shields are shown in figure 9 and 10 respectively. Similarly, in figure 11 and 12 results are reported in case of imposed temperature. One can see from the figures that a non uniform temperature field is obtained, with the minimum value occurring at the cold head surface and equal to 77.465K; it makes possible an average value of the shield equal to 80K. Similar results are obtained for the internal shield where the minimum value is equal to 16.13K (in the region of contact surface with the cold head) and the mean temperature of the shield is equal to 19.99, as desired. With regard to figures 11 and 12, one can see that the cold region temperature is equal to 80K (for the external shield) and to 20K (for the internal one); the mean temperature of the shield is in this case equal to 82.36K and 23.59K respectively, since the heat fluxes removed by the refrigerating stages result 4.69W and 3.408W. It imply that the heat flux entering the helium vessel is 0.022W, a double value with respect to the previous case. In any case, this almost uniform temperature field is due to the high value of thermal conductivity of the aluminum shields (about 200÷240 W/mK).

3.4 Zero Boil Off system

The Zero Boil Off configuration, with a temperature of second stage equal to about 4K, allows the condensation inside the vessel of helium that could be evaporated, eliminating helium consumption. The first stage of the cold head, in this case, helps to refrigerate a single shield at 50K. Thus, cryostat is composed by three vessels, missing one aluminum shield. Heat fluxes obtained in this case are reported in Table 4.

Table 4. Thermal fluxes.

Surfaces	Radiative fluxes $[W]$	Specific radiative fluxes $\left[\frac{W}{m^2}\right]$	Mean temperature $[K]$
External surface external steel vessel	-2.79	-0.11	293.05
Internal surface external steel vessel	6.84	0.27	293.05
External surface DAM	-6.82	-0.27	246.81
Internal surface DAM	6.82	0.28	246.67
External surface alu vessel	-6.8	-0.28	50
Internal surface alu vessel	0.44	0.018	50
External surface internal steel vessel	-0.44	-0.019	4.2
Internal surface internal steel vessel	0	0	4.2

Thermal fields obtained with imposed heat flux to the stages of the cold head are shown in figure 13 and figure 14.

Figure 9. Temperature field on external aluminum shield (imposed heat flux).

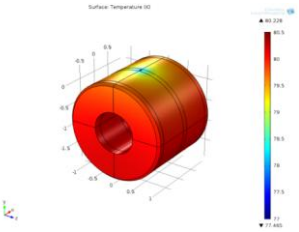

Figure 10. Temperature field on internal aluminum shield (imposed heat flux).

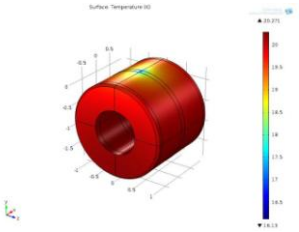

Figure 11. Temperature field on external aluminum shield (imposed temperature).

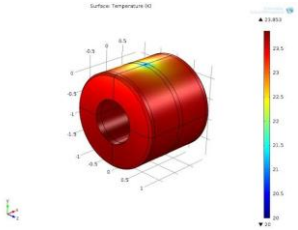

Figure 12. Temperature field on the internal aluminum shield (imposed temperature).

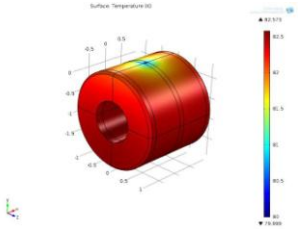

Figure 13. Temperature field on external aluminum shield (imposed heat flux).

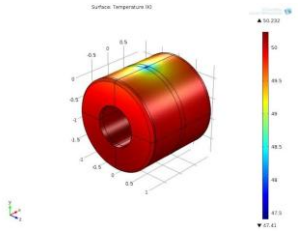

Figure 14. Temperature field on internal helium vessel (imposed heat flux).

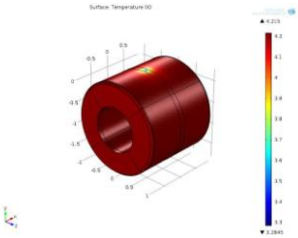

The minimum and mean values of temperature are equal to 47.41K and 50K for the cryo-shield and 3.28K and 4.2K for helium vessel.

3.5 Simulations with tie-rods

Since the architecture of real cryostats implies the mounting of tie rods that allow to maintain the empty cavity and to center the magnetic field, thermal field has been evaluated in case of tie rods mounted. For these simulations we used a geometry with flat closures and we inserted tie-rods among vessels of the cryostat.

Each vessel contains 4 tie-rods which fix it on the opposite one.

Table 5. Properties of different vessels

Vessel	Volume $[m^3]$	Density $\left[\frac{Kg}{m^3}\right]$	Mass $[Kg]$
External Steel	0.119	7999.5	951.94
External Aluminum	0.155	2712.6	420.45
Internal Aluminum	0.097	2712.6	263.12
Internal Steel	0.145	7999.5	1159.92

For MRI machines, tie-rods are made of fiber glass because this material achieves a mechanical resistance near to theoretical resistance of the covalent bond.
Since tie-rods provide a conductive way for heat among the vessels, they pertly affect heat transfer and thermal field. In Figure 15 and 16 temperature fields are shown for external aluminium vessel and external steel vessel respectively in case of imposed heat flux.

Figure 15. Thermal field on external aluminum vessel with fiber glass tie-rods

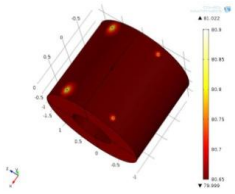

Figure 16. Thermal field on external steel vessel with fiber glass tie-rods

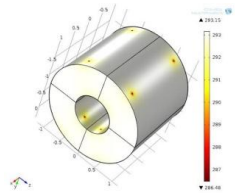

Figure 16 and 17 show the temperature field along tie rods.
It can be noted that the temperature value at the end of the tie-rod, in contact with the external steel, is lower than the average temperature of the vessel (equal to 293.1 K).
This has no significant effect on external steel vessel and external aluminum vessel (Figure 15).

Figure 17. Temperature field along fiber glass tie-rod inserted between external steel vessel and internal aluminum vessel

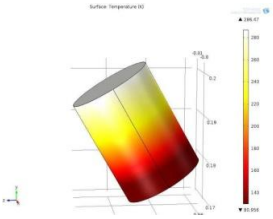

Figure 18. temperature field along fiber glass tie-rod in contact with internal steel vessel containing liquid helium.

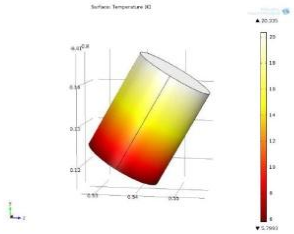

For internal steel vessel this effect is not negligible since the temperature value at the contact points with tie-rods reaches a value of 5.79 K so the liquid helium evaporates very quickly.

Additional simulations have been performed with stainless steel tie-rods to better understand the conductive effect of different internal conductivity values. Local temperatures values achieves in this case 15 K, causing the quench of magnet.

this preliminary results suggest the need to evaluate the choice of different materials for the tie rods.

4. Conclusions

Preliminary results related to the description of thermal field in a cryostat for nuclear magnetic resonance imaging have been presented, starting with a three-dimensional geometric model of the cryostat. Resulting heat flux entering in 80K cryo-shield without DAM's sheet is too high and not sustainable by any commercial cold head. Two boundary conditions have been analyzed to simulate the effect of the cold head. The imposed heat flux boundary condition provides a thermal field for which the overall cooling of the two shields at the desired temperature is ensured. Finally, zero-boil off system have been simulated with helium vessel maintained at 4K; resulting heat flux entering in cryo-shield and vessel wall is sustainable by cold head. with regard to tie rods, the choice of material is crucial to maintain the empty cavity and avoid the quench of

magnet; next simulations will concern more realistic geometrical and mechanical configurations.

5. Acknowledgments

The authors thank Prof. Francesco Paolo Branca for constructive comments and helpful suggestions and for making available the NMR tomography.

6. References

[1] J.Bardeen, L.N.Cooper, and J.R.Schrieffer, Theory of Superconductivity, Phys. Rev.108, 1175 (1957).
[2] Lehmann G. e Mangano R. "Pulse Tube cryocooler system for magnetic resonance superconducting", Justia Patent nr. 6807812.
[3] www.siemens.com.
[4] Churchill, S. W., and Chu, H.H.S., 1975, "Correlating Equations for Laminar and Turbulent Free Convection from a Vertical Plate," Int. J. Heat Mass Transfer, Vol. 18, pp. 1323-1329.
[5] F.P. Incropera and D.P. DeWitt, Fundamentals of Heat and Mass Transfer, fifth ed. John Wiley & Sons, 2002.